Journal of MATERIALS RESEARCH

Invited Feature Paper
DOI:10.1557/s43578-023-01173-9

EARLY CAREER SCHOLARS IN MATERIALS SCIENCE, 2024

Influence of PMMA particle size control on the transmittance of PMMA/tempo-oxidized cellulose composites

Julia P. Altarugio[1], Lucas H. Staffa[2], Antonio J. F. Carvalho[1], Juliana M. P. Almeida[1,2,a)]

[1] São Carlos School of Engineering (EESC), University of São Paulo (USP), São Carlos, SP 13563-120, Brazil
[2] Department of Materials Engineering (DEMa), Federal University of São Carlos (UFSCar), São Carlos, SP 13565-905, Brazil
[a)] Address all correspondence to this author. e-mail: juliana.almeida@ufscar.br

Received: 14 June 2023; accepted: 20 September 2023

Cellulose is a class of biopolymers that prominently contributes to developing lightweight, eco-friendly, and biodegradable plastics. Among them, nanofibrillated cellulose (NFC) is one of the most interesting due to its mechanical behavior. Mixing it with synthetic plastic such as poly(methyl methacrylate) (PMMA) reduces synthetic polymer usage, agro-industrial residue and develops fiber-reinforced composites. NFC was prepared from residual biomass and oxidized with TEMPO (2,2,6,6-tetramethylpiperidine-1-oxyl radical). Herein, NFC was incorporated (25, 50 and 75 wt%) in a colloidal emulsion of PMMA, with PMMA particle size control (50 and 175 nm). The investigation of this system on the PMMA/NFC transparency was addressed here. FTIR and SEM demonstrated effective incorporation of NFC and interaction with the PMMA. The increment of NFC increased the water contact angle and improved film transparency. Paired with PMMA particle size control, particularly at 50 nm, this favored composite transparency, becoming close to or even greater than pure NFC.

Juliana M. P. Almeida

Juliana M. P. Almeida is an Assistant Professor at the Department of Materials Engineering of Federal University of São Carlos (UFSCar), developing research on Laser Material Processing, Optical glasses and Ionic Superconductors. Juliana M. P. Almeida received her B.S. in Natural Science with an emphasis in Physics in 2009 at University of São Paulo (USP). Continuing her research devoted to femtosecond laser writing, optical waveguides and nonlinear optical spectroscopy, Dr. Almeida also received her MS from USP in 2011, and her Ph.D from USP in 2015. Between 2013 and 2014, she was Visiting Student Research Collaborator at Princeton University, extending her research to amorphous chalcogenides, focusing on optical and structural characterization techniques. Dr. Juliana M. P. Almeida carried out post-doctorate research on Laser Induced Forward Transfer of glasses, polymers and metals; on piezophotonic ceramics and block copolymer lithography.

Introduction

Cellulose is a natural linear homopolymer that can be obtained from plant fibers and is the most abundant biopolymer available [1]. In addition to being a biodegradable and low-cost material, it has great mechanical properties, which makes the use of cellulose interesting as a technological, biodegradable, and sustainable material [2, 3].

One large source of lignocellulosic material, particularly cellulose, is sugarcane bagasse. In Brazil, sugarcane stands as a prominent primary resource for the agricultural industry [4]. Its bagasse resulting from sugar and alcohol production corresponds to 30% of the total cane crushed, which in the 2019/2020 season corresponded to 192 tons of bagasse [5]. Using this residual biomass to extract cellulose for the

development of multicomponent material is an alternative to minimizing the agro-industrial residues. Besides, cellulose's structure possesses the inherent potential to undergo chemical or mechanical modifications in order to achieve properties that are desirable according to its specific application and intended use.

A relevant structure modification of cellulose is microfibrillated cellulose (MFC), obtained from significantly or partially fibrillated natural fibers [6]. MFC presents high crystallinity and a diameter range of 20-100 nm with a length of a few tens of micrometers [7]. These aforementioned characteristics provide high mechanical strength and remarkable barrier properties and allow structural modifications through chemical reactions [8].

In order to proceed with further structural modification aiming at the development of nanofibrillated cellulose, there is the regioselective oxidation of cellulose mediated by 2,2,6,6-tetramethylpiperidine (TEMPO) in a mild aqueous environment. In this reaction, it is possible to convert C6 primary hydroxyl into aldehyde and carboxyl groups, in addition to attributing negative charges to the cellulose. This results in helpful properties, such as improvement of hydrophobicity, UV-light blocking, transparency, and haze for visible light [6, 9, 10]. TEMPO-oxidized cellulose has been investigated in epoxy laminates and polystyrene (PS) matrix to design renewable high-performance composite materials [11, 12]. Composites of TEMPO-oxidized cellulose nanofibrils (TOCNs) and polystyrene were developed, maintaining good transparency even with 10 wt% of TOCN. In addition, due to TOCN's distinctive characteristics such as high crystallinity and aspect ratio, this composite presented an exceptional reinforcement effect [12].

Poly(methyl methacrylate) (PMMA) is a visible-light transparent synthetic polymer that can be used as a substitute for inorganic glass since its discovery on account of its transparency, high impact strength, dimensional stability, and weather resistance [13]. Nowadays, worldwide spread applications of PMMA range from packaging to biomedical implants [14], optic [15], cosmetic, and construction materials [16]. In addition to these applications, PMMA can be used for the development of multicomponent polymeric material via the incorporation of inorganic fillers, such as carbon nanotubes [17], clays [18], metals, and semiconductor particles [19, 20]. This approach has allowed new PMMA functionalization, with the potential for electrolytes, electronic packaging, and optoelectronic devices.

Although some inorganic fillers can improve or modify numerous properties of PMMA, its transparency is generally impaired, besides the toxicity of some inorganic particles [21, 22]. In addition, the ability to retain good transparency of PMMA when mixing it with other materials demands a good distribution and uniform dispersion of the dispersed phase, avoiding agglomerations [23] and a good control of emulsion polymerized PMMA particle size. This context strengthens the fact that the search for modifying the properties of PMMA while maintaining its visible-light transparency still sustains research efforts.

Due to this large variety of applications, the use of PMMA and its composites has been growing, and it is crucial to reduce fossil-based materials [24]. Research endeavors continue to be supported for the utilization of cellulose-based materials as reinforcement in polymer matrices [25]. An efficient alternative is mixing it with natural polymers generating a material that contains less synthetic polymer and driving the incorporation of renewable carbon sources [25, 26].

Compounds can be obtained from synthetic materials and, at the same time, are more susceptible to biodegradation due to the addition of natural polymers [27, 28]. For instance, starch and cellulose have been the most useful natural polymers for the development of lightweight environmentally friendly biodegradable plastics [29, 30] [31]. In particular, the addition of lignocellulosic fibers is interesting not only for the reduction of synthetic polymer but also due to the advantages of fiber-reinforced composites [32].

Within this specific context of developing transparent multicomponent polymeric materials, cellulosic-based materials have already been used as a reinforcing material for optically transparent polymers [23, 33]. For instance, PMMA has already been combined with microcrystalline cellulose (MCC) by the solution casting method. The resulting composites demonstrated good visible-light transparency due to the particle size control and good dispersion of the MCC in the polymeric matrix [23]. Another example was the development of composites based on networks of nanofibrillated bacterial cellulose and acrylic and epoxy resins. This approach reinforced synthetic polymeric resins and maintained the original resin's visible-light transparency, demonstrating great potential in the elaboration of optically functional multicomponent materials [33].

Although the preparation and characterization of transparent PMMA/cellulose-based composites has already been explored in the literature [2, 23, 33], it is essential to address further investigation and attention regarding the incorporation of TEMPO-oxidized nanofibrillated cellulose into PMMA emulsion with PMMA particle size control and the subsequent implications in the PMMA/NFC composite visible-light transparency. In our best knowledge, this approach has not yet been addressed in the literature.

Considering the interest to reduce inorganic fillers, allied with the advantages of incorporation of vegetal fibers in acrylic polymers, this study aimed to develop TEMPO-oxidized cellulose/PMMA transparent composite films. The films were prepared by mixing NFC and emulsion polymerized PMMA with different PMMA particle sizes (50 nm and 175 nm) and NFC content (25, 50 and 75%wt), allowing for reduction not only

synthetic polymer usage but also the agro-industrial residue. Efforts here are also based on maintaining PMMA transparency, aiming at PMMA particle size and NFC content control, and an adequate distribution and uniform dispersion of NFC in the composite. PMMA particle size control was performed during its synthesis using a biodegradable surfactant.

Results and discussion

PMMA was synthesized via emulsion polymerization, an experimental arrangement that consists of water, a poorly water-soluble monomer (methyl methacrylate–MMA), a water-soluble radical-generator initiator (potassium persulfate), and a surfactant (SDBS) [34]. During the polymerization process, the formed polymer organizes itself in the form of small spherical particles.

Analyzing the surfactant (SDBS) amount's influence in PMMA emulsion is relevant because it changes the particle size and particle size distribution and directly affects the optical properties. Figure 1 exhibits the particle diameter distribution obtained by DLS analysis.

The average hydrodynamic diameter for the investigated emulsions is indicated on the respective curves. The particle size distribution is nearly monomodal, suggesting there are no significant agglomerations among the PMMA particles [35]. Furthermore, one can note that the concentration of SDBS changed PMMA particle diameter from 50 to 175 nm. Moreover, it is noted that the increase in the SDBS content causes a decrease in the PMMA particle size. Considering it, emulsions containing the smallest and largest particle diameters (Emulsion 1 and 3, respectively) were selected for subsequent steps, *i.e.*, mixing with different amounts of NFC (25, 50, and 75%wt).

Figure 2 shows the FTIR spectra of the composite films made with the smallest PMMA particles (50 nm), along with neat PMMA and neat NFC film for comparison. Composite films containing a PMMA particle size of 175 nm (the largest PMMA particle size emulsion) were also analyzed and showed a similar behavior (not displayed in the figure). FTIR measurements were performed to analyze PMMA incorporation into cellulose.

PMMA presents characteristic fingerprint bands at 750, 842, 987, 1242, and 1727 cm^{-1}, corresponding to the skeletal C–C vibrations, $-CH_2$, $O-CH_3$ coupled with γ(COC), γCCO, and C = O stretching mode, respectively. It is important to note that these bands are absent in pure NFC film. In the NFC FTIR spectrum, the remarkable band at 1600 cm^{-1} is associated with the formation of COOH groups from the oxidation of cellulose due to the regioselective oxidation mediated by TEMPO. This band may be attributed to C=O bonds due to the absorbed humidity by carbonyl groups [36]. In addition, one can highlight 1158 cm^{-1} for γCOC at β-glucosidic linkage and 1202 cm^{-1} for δCOH in plane at C6 [37].

The presence of 750, 1727, and 1600 cm^{-1} vibrational bands in S25, S50, and S75 spectra in Fig. 2 demonstrate that cellulose was incorporated in PMMA for the whole compositional range, as corroborated by microscopy analyses in Fig. 3.

Optical microscopy (OM) and Scanning Electron Microscopy (SEM) images are displayed in Fig. 3. Here, the objective was to observe the composite's morphology and the interaction between its phases. Although S25 film contains particles 3.5 times smaller than L25 film, no difference in film microstructure was seen through optical images, as presented in Fig. 3(a) and (b). Moreover, it is possible to note residual microfibers of cellulose that were not converted into nanofibers.

Due to the nanometer size of PMMA particles, it was not possible to see this phase via OM. Nonetheless, such features

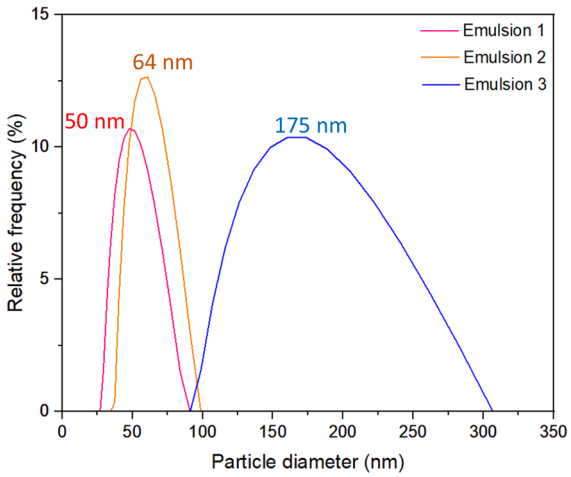

Figure 1: Particle size distribution obtained via DLS analysis for each PMMA emulsion.

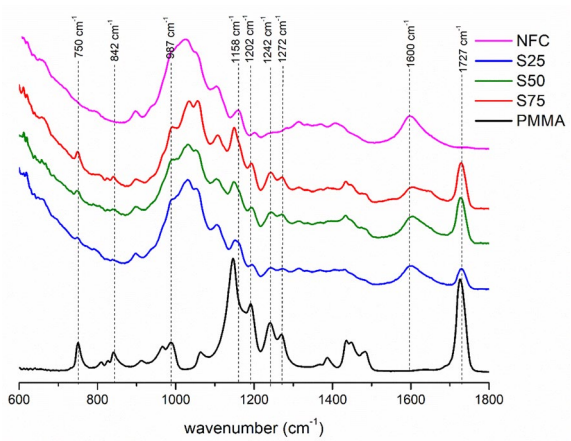

Figure 2: FTIR spectrum of the neat PMMA and NFC and NFC/PMMA films.

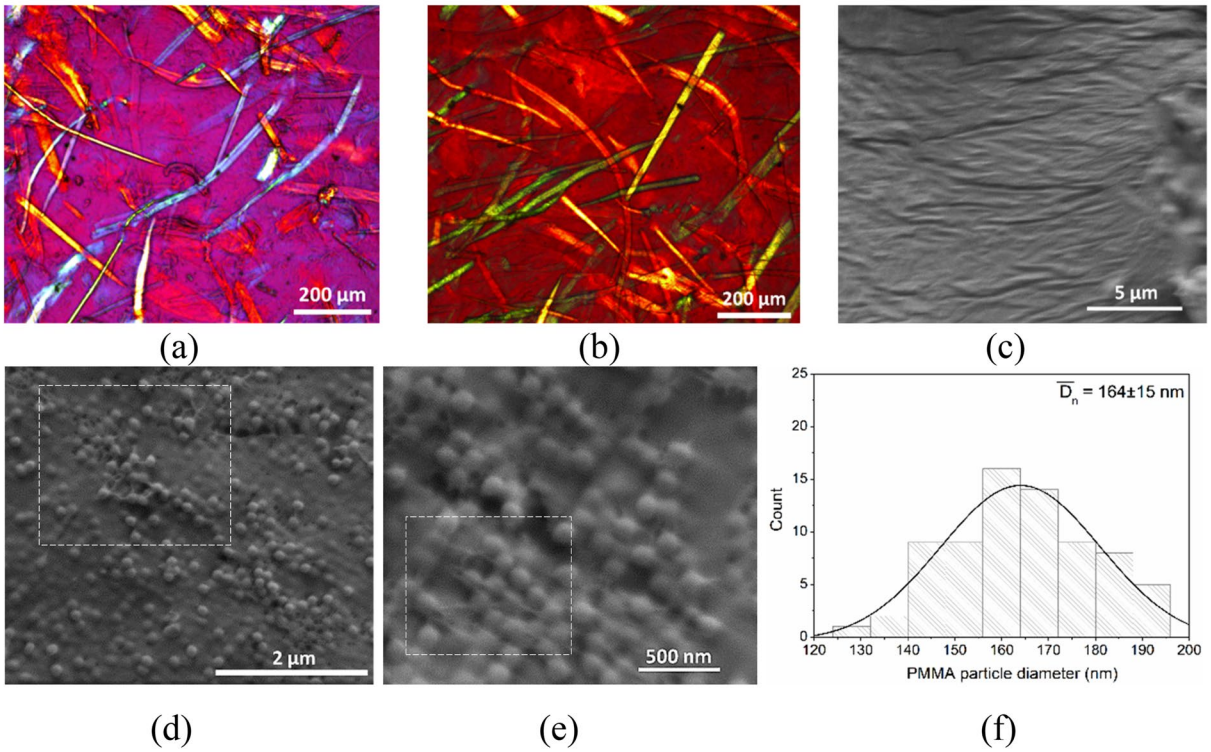

Figure 3: Optical microscopy (OM) analyses of (a) S25 and (b) L25. Scanning Electron Microscopy (SEM) analysis of (c) pure NFC, (d) L25, and (e) L25 with higher magnification and particle size distribution of (f) L25. The highlighted area refers to PMMA and NFC interactions.

can be seen in Fig. 3(c) and (d), which displays a SEM image of L25 film demonstrating a homogeneous distribution of nanometer PMMA spheres and good fiber dispersion. In addition, the average PMMA particle size determined via SEM [Fig. 3(c) and (d)] using Image J software was 164 ± 15 nm. This value is close to the hydrodynamic particle diameter determined via DLS for emulsion 3 (Fig. 1).

Furthermore, the highlighted area indicates the bonding between PMMA particles and NFC, generating a network between these two phases. It is suggested that PMMA particles shows a good adhesion to NFC fibrils due to its polar character, such as hydrogen bonds between NFC hydroxyl groups and MMA carbonyl groups [38].

Figure 4 presents thermogravimetric analysis (TGA) and the derivative curve (DTG) of S25 and L25, in order to verify the effect of PMMA particle size on the composite decomposition profile. Both TGA curves demonstrate two major mass loss stages besides the initial range (< 200 °C) that show a loss of 6% corresponding to the elimination of surface water. Between 240 °C and 300 °C occurs NFC decomposition due to hemicellulose depolymerization and the cleavage of glycosidic linkages [39]. The maximum mass loss at this stage was observed at around 275 °C, and the total mass loss was 32%, close to the NFC amount in the composite film. Between 350 °C and 450 °C occurs the decomposition of the acrylic phase with a total mass

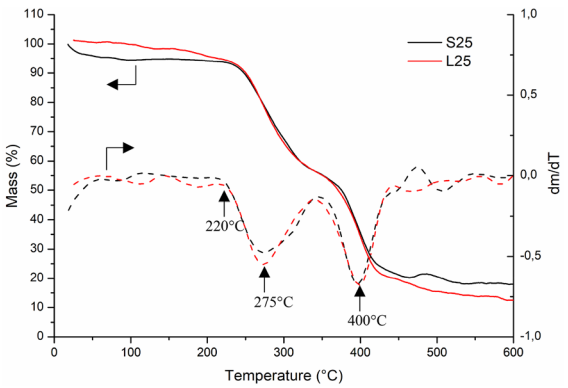

Figure 4: Thermogravimetric analysis of S25 and L25 films.

loss of 40%, which reached the maximum rate at around 400 °C. Above 450 °C begins the thermic decomposition of the remaining carbon. Reaching 600 °C, the films showed residual masses of 16% for S25 and 20% for L25, corresponding to the carbonaceous residues [40]. The data in Fig. 4 show that PMMA particle size does not affect film decomposition temperature, which remains stable up to around 220 °C, in which NFC decomposition processes start more significantly (as marked on the curve).

In order to study the effect of PMMA particle size and NFC content in the composite hydrophilicity, static water contact

TABLE 1: Water contact angle measurements of pure NFC film and NFC/PMMA films.

NFC content (wt%)	Water contact angle (°)	
100 (neat NFC)	51.3 ± 0.1	
	Emulsion 1	Emulsion 3
	50 nm PMMA particle size	175 nm PMMA particle size
25	53.2 ± 0.2	51.4 ± 0.1
50	44.1 ± 0.1	53.7 ± 0.2
75	45.7 ± 0.1	55.7 ± 0.1

angle measurements were performed. The values are summarized in Table 1. Each film was tested, including the neat NFC as a reference. NFC and PMMA are inherent hydrophilic materials with a water contact angle of 51.3° and 67.8° [41], respectively. Although all films presented contact angles similar to neat NFC, in general, the composite films prepared with the smallest PMMA particles displayed water contact angles smaller than the ones prepared with the largest particle size. Furthermore, with the exception of S25, a tendency to increase water contact angle can be observed with the increase of NFC content.

Kord et al. studied this phenomenon on poly(vinyl alcohol) (PVA)/NFC composite films. They reported that adding NFC improves their hydrophobicity due to strengthened inter-component hydrogen bonding, *i.e.,* the hydrogen bonding between NFC and the polymer matrix may disfavor the hydrogen bonds for water molecules, enhancing the contact angle of the films [42] (Table 1).

In order to verify the degree of visible-light transparency of the composites, UV–vis transmittance spectra were determined. Figure 5(b) and (c) shows the transmittance spectra of the films at a wavelength range of 200–800 nm. For comparison, it was analyzed NFC pure film. The results reveal that the S25, S50, and S75 films present higher transmittance at visible wavelengths, demonstrating less visible-light scattering. On the other hand, for L25, L50, and L75 there was a remarkable reduction in transmittance, especially in the region below 500 nm, which can be associated with the higher visible-light scattering by the larger PMMA particles, which sizes are closer to the light wavelength range. Figure 5(a) shows a photograph of a pure NFC film and the composite films prepared with the smallest (S25, S50, and S75) and largest (L25, L50, and L75) PMMA particles, containing 25, 50, and 75%wt of NFC.

The relationship between transmittance at 800 nm and the water contact angle is displayed in Fig. 6. Through this summary graph, it is possible to verify that, except for the behavior of S25, there is a tendency to increase the contact angle as the NFC content increases. In addition, there is a tendency to increase the static water contact angle as the size of the PMMA particles increases.

Regarding transparency results, these results also show that the addition of NFC leads to an increase in transmittance and so in the film's transparency. This finding corroborates the effective distribution and uniform dispersion of NFC in the PMMA

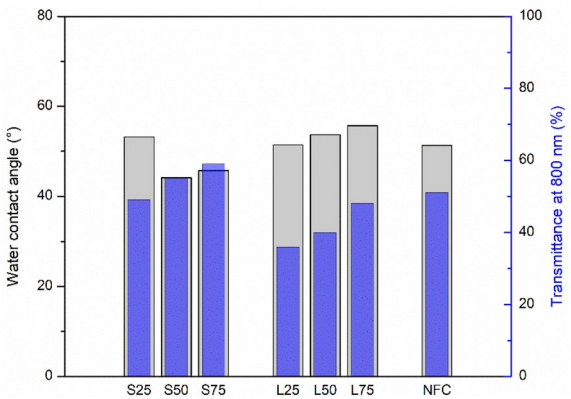

Figure 6: Water contact angle and transmittance at 800 nm of NFC/PMMA films.

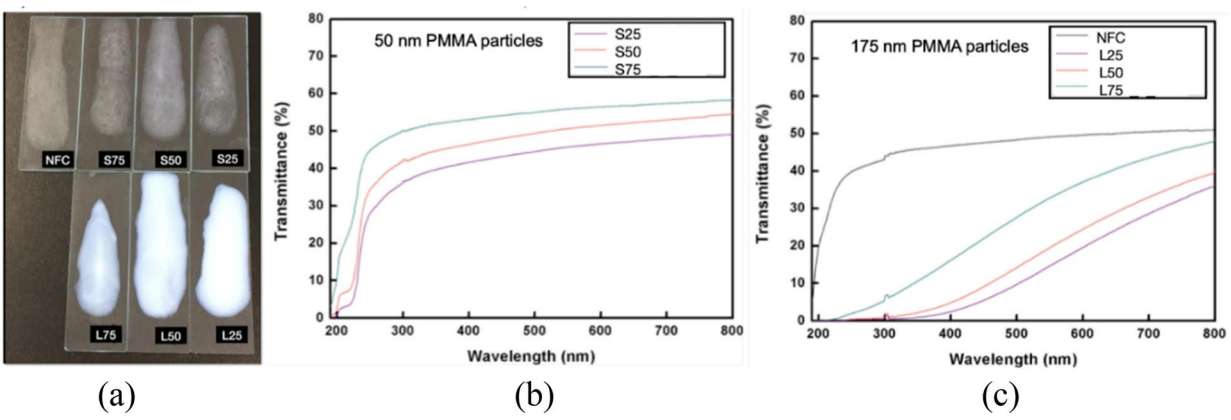

Figure 5: (a) Photograph of pure NFC film and NFC/PMMA films; (b) UV–vis transmittance spectra for the NFC/PMMA films with smaller (b) and bigger PMMA particle size (c).

matrix since the optical transmittance strongly depends on the distribution and agglomeration of cellulose nanofibers in the polymeric matrix [23]. In addition, it demonstrates the higher transmittance of the smaller PMMA particle size composite films.

The material that showed the highest transparency at 800 nm was S75. In this sample, an appropriate distribution and uniform dispersion of NFC in the acrylic matrix was reached. In addition, an NFC optimal content and PMMA particle size control generated a multicomponent material with great transparency, close to or even greater than pure NFC.

Conclusions

Poly(methyl methacrylate)/TEMPO-oxidized nanofibrillated cellulose (PMMA/NFC) composite films with different PMMA particle sizes (50 and 175 nm) were successfully prepared adding NFC at 25, 50, and 75%wt concentrations. The variation of PMMA particle sizes from 50–175 nm was obtained by modifying the amount of SDBS surfactant during emulsion polymerization.

SEM analysis showed that PMMA particles were homogeneously distributed in the NFC/PMMA film and bonded to NFC. In addition, the PMMA particle size is close to the average hydrodynamic particle diameters determined via DLS.

FTIR analysis indicated the PMMA/NFC films had fingerprints of both components suggesting effective incorporation, while TGA demonstrated similar thermal behavior between the composites, regardless of the PMMA particle size. Water contact angle analysis showed that all films presented a hydrophilic characteristic, with static water contact angles between 44.1° and 55.7°. In addition, there is a tendency of increasing static water contact angle as the NFC content is increased.

Moreover, a proper distribution and uniform dispersion of NFC, in addition to PMMA particle size control and NFC content, are essential for the visible-light transparency of the composite film. The smaller the PMMA particle size, the more transparent the film. Furthermore, UV–vis light transmittance demonstrated that, by increasing the NFC content in the composite, there is an increase in transmittance at 800 nm, *i.e.,* in the composite film transparency.

Materials and methods

Preparation of PMMA emulsions

PMMA emulsions with different particle sizes were prepared by emulsion polymerization using a dispersion of 71.2 g of methyl methacrylate monomer (Merck) in 150 mL of distilled water, 200 mg of initiator potassium persulfate (Synth) dissolved in 31.4 mL of water, and different contents of sodium dodecylbenzenesulfonate (SDBS) surfactant in 100 mL of water. The mixture of these was added to a glass reactor equipped with a mechanical agitator (~ 600 rpm) and kept in a thermostatic bath at 85 °C for 4 h. Three emulsions were prepared, and they are displayed in Table 2.

TABLE 2: Identification and SDBS amount used for the preparation of PMMA emulsion with different particle sizes.

	SDBS (g) in 100 mL of water
Emulsion 1	3.5
Emulsion 2	1.5
Emulsion 3	0.015

Preparation of NFC

NFC was extracted from the sugarcane bagasse following the process described by Grande et al. [4]. This process consists of washing the bagasse with hot water, bleaching, and sonication of the bagasse fibers.

Briefly, this process consisted of pre-extraction of the bagasse with a toluene/ethanol solution (2:1 v/v) for 8 h. This extracted bagasse was dried at room temperature for 4 h and then in an oven at 75 °C for 1 h. This was followed by bleaching with a sodium chloride solution, in which the fibers were dispersed in an aqueous solution of 1.3% NaCl pH ~ 4. The mixture was poured into an Erlenmeyer flask connected to a reflux condenser and kept at 75° C under magnetic stirring for 1 h. After this period, the suspension was filtered under reduced pressure. Then, the hemicellulose was extracted with a KOH solution at 85 °C (5 g of KOH and 250 mL of distilled water) under stirring for 2 h. This fiber was filtered and washed with distilled water until neutral pH. This procedure was repeated twice, and then the fibers were dispersed in 200 mL of distilled water and cooled in an ice bath. Before the sonication process, part of the obtained material was oxidized using 2,2,6,6-tetramethylpiperidine (TEMPO) (0,1 mmol/g) and sodium bromate (1 mmol/1 g cellulose) [43]. This material was agitated for 2 h at room temperature, and the pH value of 10.5 was maintained by adding NaOH. After that, the material was washed with deionized water and had the pH neutralized with HCl. Finally, ultrasound sonification (Hielscher-UP400S) was performed. An ice bath was used to avoid heating the sample. The optimized sonication condition consisted of a total time of 40 min, with pulses applied for 10 s.

Preparation of the films

Films were prepared by mixing PMMA emulsions with different amounts of NFC (25, 50, and 75%wt) and distilled H_2O (0,5 mL/g NFC), used as a solvent. In this stage, emulsions 1 and 3 were chosen for providing the smallest and the largest PMMA

TABLE 3: Composition of the prepared NFC/PMMA films.

Samples	PMMA emulsion used	NFC content in the film (%wt)
S25	Emulsion 1 50 nm PMMA particle size	25
S50		50
S75		75
L25	Emulsion 3 175 nm PMMA particle size	25
L50		50
L75		75

particle sizes (50 and 175 μm). After magnetic stirring, the mixture was cast on glass microscope slides and leveled using a fixed height of 1 mm, adjustable with micrometers on the film applicator by doctor blade technique. The films were allowed to dry at ambient conditions. Table 3 summarizes the preparation features of the films, along with their sample identification.

Characterization techniques

Dynamic Light Scattering (DLS) analyses were performed using Litesizer 500 to determine the average hydrodynamic particle diameters and the polydispersity index of PMMA emulsions. This technique was used to characterize the hydrodynamic diameter distribution only in the PMMA emulsions, measuring the random changes in the intensity of light scattered. All further analyses were performed for the film specimens.

Optical microscopy (OM) and Scanning Electron Microscopy (SEM), using Leica DM2700 (OM) and Inspect F50 microscopes (SEM-FEG), respectively, were performed in order to check film homogeneity in terms of aggregates, *i.e.,* distribution and dispersion of NFC, besides the interaction between NFC and PMMA particles. Chemical structure characterization was carried out by FTIR analysis using Spectrum 100 (Perkin-Elmer), with spectra acquired between 1800 and 600 cm^{-1} and 4 cm^{-1} of resolution at ATR mode. For this characterization, it was also analyzed the pure films of NFC and PMMA for comparative reasons.

Thermal stability was investigated by thermogravimetric analysis (TGA) using Pyris 1 (Perkin-Elmer) under a nitrogen atmosphere (20 mL min^{-1}). The analysis was performed under non-isothermal conditions, from 25 °C to 600 °C, at a heating rate of 10 °C/min. Smoothed TG and DTG curves were reported here.

Wettability was evaluated by water static contact angle using a KSV CAM 200 equipment at 25°C. The water contact angle values correspond to an average of 2 measurements and stabilization time from 0 to 0.6 s. The optical transmittance of the films was measured using a UV–VIS spectrophotometer (Bel Photonics, UV-M51) at wavelengths from 200 to 800 nm.

Acknowledgments

This study was financed in part by the Coordenação de Aperfeiçoamento de Pessoal de Nível Superior—Brasil (CAPES)—Finance Code 001. This work has also been supported by the following Brazilian research agencies: FAPESP and CNPq. AJFC thanks to CNPq Proc. No. 303847/2019-0.

Data availability

The authors declared that all the data supporting the findings are available within the paper.

Declarations

Conflict of interest The authors declare no conflict of interest related to this research work. This manuscript was not under consideration by any other journal.

Open Access

References

1. C. Ma, C. Xu, Q. Meng, H. Yang, R. Xie, H. Zhang, H. Tu, Y. Zhao, M. Wang, G. Xu, J. Zhu, J. Mater. Res. **37**(18), 3049–3059 (2022). https://doi.org/10.1557/s43578-022-00710-2
2. E.E. Kiziltas, A. Kiziltas, S.C. Bollin, D.J. Gardner, Carbohyd. Polym. **127**(20), 381–389 (2015). https://doi.org/10.1016/j.carbpol.2015.03.029
3. S.J. Horn, G. Vaaje-Kolstad, B. Westereng, V.G.H. Eijsink, Biotechnol. Biofuels **5**(1), 45 (2012). https://doi.org/10.1186/1754-6834-5-45
4. R. Grande, E. Trovatti, M.T.B. Pimenta, A.J.F. Carvalho, J Renew. Mater. **6**(2), 195–202 (2018). https://doi.org/10.7569/JRM.2018.634109
5. W.F.D.P. Bezerra, G. Dognani, L.N. Alencar, M.P.S. Parizi, R.F. Boina, F.C. Cabrera, A.E. Jon, Materia (2022). https://doi.org/10.1590/S1517-707620220001.1342

6. S. Liu, Z.X. Low, Z. Xie, H. Wang, Adv. Mater. Technol. **6**(7), 2001180 (2021). https://doi.org/10.1002/admt.202001180
7. I. Siró, D. Plackett, Cellulose **17**(3), 459–494 (2010). https://doi.org/10.1007/s10570-010-9405-y
8. H. Chen, B. Wang, J. Li, G. Ying, K. Chen, Carbohyd. Polym. **288**(15), 119371 (2022). https://doi.org/10.1016/j.carbpol.2022.119371
9. C. Lin, Q. Wang, Q. Deng, H. Huang, F. Huang, L. Huang, Y. Ni, L. Chen, S. Cao, X. Ma, Cellulose **26**, 4061–4069 (2019). https://doi.org/10.1007/s10570-019-02367-3
10. Z. Fang, H. Zhu, W. Bao, C. Preston, Z. Liu, J. Dai, Y. Li, L. Hu *Energy*. Environ. Sci. **7**(10), 3313–3319 (2014). https://doi.org/10.1039/c4ee02236j
11. K. Lee, G. Kwon, Y. Jeon, S. Jeon, C. Hong, J.W. Choung, J. You Carbohyd. Polym. **291**, 119514 (2022). https://doi.org/10.1016/j.carbpol.2022.119514
12. S. Fujisawa, T. Ikeuchi, M. Takeuchi, T. Saito, A. Isogai, Biomacromol **13**(7), 2188–2194 (2012). https://doi.org/10.1021/bm300609c
13. U. Ali, K.J.B.A. Karim, N.A. Buang, Polym. Rev. **55**(4), 678–705 (2015). https://doi.org/10.1080/15583724.2015.1031377
14. J.H. Wu, M.S. Yen, C.W. Chen, M.C. Kuo, J. Polym. Environ. **24**(4), 318–327 (2016). https://doi.org/10.1007/s10924-016-0775-6
15. L.H. Lee, W.C. Chen, Chem. Mater. **13**(3), 1137–1138 (2001). https://doi.org/10.1021/cm000937z
16. S.M. El-Bashir, A. Hendi, Polym.-Plast. Technol. **49**(1), 78–82 (2010). https://doi.org/10.1080/03602550903283075
17. J.K. Abraham, B. Philip, A. Witchurch, V.K. Varadan, C. Channa Reddy, Smart Mater. Struct. **13**(5), 1045–1049 (2004). https://doi.org/10.1088/0964-1726/13/5/010
18. M. Deka, A. Kumar, Electrochim. Acta **55**(5), 1836–1842 (2010). https://doi.org/10.1016/j.electacta.2009.10.076
19. N. Singh, P.K. Khanna, Mater. Chem. Phys. **104**(2–3), 367–372 (2007). https://doi.org/10.1016/j.matchemphys.2007.03.026
20. P. Maji, R.B. Choudhary, M. Majhi, Appl. Phys. A-Mater. (2018). https://doi.org/10.1007/s00339-017-1487-z
21. X. Wu, Y. Gao, H. Yao, K. Sun, R. Fan, X. Lo, Y. An, Y. Lei, Y. Zhang, J. Appl. Polym. Sci. **137**(28), 448864 (2020). https://doi.org/10.1002/app.48864
22. Y. Kahraman, H. Gursu, M.B. Arvas, M.G. Ersozoglu, M. Nofar, A.S. Sarac, Y. Sahin, J. Appl. Polym. Sci. **139**(36), e52828 (2022). https://doi.org/10.1002/app.52828
23. H. Liu, D. Liu, F. Yao, Q. Wu, Bioresour. Technol. **101**(14), 5685–5692 (2010). https://doi.org/10.1016/j.biortech.2010.02.045
24. X. Yu, Bio-based polymers: a mini review. ChemRXiv (2022). https://doi.org/10.26434/chemrxiv-2022-1bnrm
25. S. Villegas-Villalobos, L.E. Díaz, G. Vilariño-Feltrer, A. Vallés-Lluch, J.A. Gómez-Tejedor, M.F. Valero, J. Mater. Res. **33**(17), 2598–2611 (2018). https://doi.org/10.1557/jmr.2018.286
26. Y.N. Sudhakar, M. Selvakumar, D.K. Bhat, Polym. Bull. **80**, 5623–5639 (2022). https://doi.org/10.1007/s00289-022-04319-7
27. D.K. Bhat, M.S. Kumar, J. Polym. Environ. **14**(4), 385–392 (2006). https://doi.org/10.1007/s10924-006-0032-5
28. Y. Zhang, W. Wang, F. Zhang, L. Huang, K. Dai, C. Li, D. Liu, Y. Sun, D. Ren, J. Wu, Q. Zheng, Carbon **189**(15), 265–275 (2022). https://doi.org/10.1016/j.carbon.2021.12.067
29. L. Di Gioia, B. Cuq, S. Guilbert, J. Mater. Res. **15**(12), 2612–2619 (2000). https://doi.org/10.1557/JMR.2000.0375
30. K. Agarwal, V. Srinivasan, V. Lather, D. Pandita, K.S. Vasanthan, J. Mater. Res. **38**(1), 112–141 (2023). https://doi.org/10.1557/s43578-022-00524-2
31. L.M. Kalossaka, A.A. Mohammed, G. Sena, L. Barter, C. Myant, J. Mater. Res. **36**(21), 4249–4261 (2021). https://doi.org/10.1557/s43578-021-00411-2
32. K.L. Pickering, M.G.A. Efendy, T.M. Le, Compos. Part A-Appl. S **83**, 98–112 (2016). https://doi.org/10.1016/j.compositesa.2015.08.038
33. H. Yano, J. Sugiyama, A.N. Nakagaito, M. Nogi, T. Matsuura, M. Hikita, K. Handa, Adv. Mater. **17**(2), 153–155 (2005). https://doi.org/10.1002/adma.200400597
34. B. Dietrich, C. Harald, R. Matthias, R. Helmut, B. Voit, *Polymer synthesis: theory and practice - fundamentals, methods, experiments*, 5th edn. (Springer-Verlag, Berlin Heidelberg, 2013)
35. M.-X. Wei, C.-H. Liu, H. Lee, B.-W. Lee, C.-H. Hsu, H.-P. Ling, Y.-C. Wu, Coatings **10**(7), 679 (2020). https://doi.org/10.3390/coatings10070679
36. H. Yuan, X. Guo, T. Xiao, Q. Ma, Y. Wu, Cellulose **26**(12), 7175–7183 (2019). https://doi.org/10.1007/s10570-019-02593-9
37. S.Y. Oh, D.I. Yoo, Y. Shin, H.C. Kim, H.Y. Kim, Y.S. Chung, W.H. Park, J.H. Youk, Carbohydr. Res. **340**(15), 2376–2391 (2005). https://doi.org/10.1016/j.carres.2005.08.007
38. F. Grüneberger, A. Huch, T. Geiger, T. Zimmermann, P. Tingaut, Colloid Polym. Sci. **294**(9), 1393–1403 (2016). https://doi.org/10.1007/s00396-016-3899-2
39. K.Y. Lee, T. Tammelin, K. Schulfter, H. Kiiskinen, J. Samela, A. Bismarck, ACS Appl. Mater. Inter. **4**(8), 4078–4086 (2012). https://doi.org/10.1021/am300852a
40. R.V. Rao, P.V. Ashokan, M.H. Shridhar, Polym. Degrad. Stabil. **70**(1), 11–16 (2000). https://doi.org/10.1016/S0141-3910(00)00055-0
41. Y. Ma, X. Cao, X. Feng, Y. Ma, H. Zou, Polymer **48**(26), 7455–7460 (2007). https://doi.org/10.1016/j.polymer.2007.10.038
42. B. Kord, B. Malekian, H. Yousefi, A. Najafi, Maderas-Ciencia y Tecnol. **18**(4), 743–752 (2016). https://doi.org/10.4067/S0718-221X2016005000065
43. T. Saito, Y. Okita, T.T. Nge, J. Sugiyama, A. Isogai, Carbohyd. Polym. **65**(4), 435–440 (2006). https://doi.org/10.1016/j.carbpol.2006.01.034